Water balance in Alpine catchments by Sentinel data

Enter authors here: R. Perico[1], P. Brunner[2], P. Frattini[1] and G.B. Crosta[1]

[1]Department of Earth and Environmental Sciences, University of Milano Bicocca, Milano, Italy.

[2]Centre for Hydrogeology and Geothermics (CHYN), University of Neuchâtel, Neuchâtel, Switzerland

Corresponding author: Roberta Perico (r.perico@campus.unimib.it)

Key Points:

- New methodology to quantify groundwater storage in snow-dominated catchments by the residual water balance approach is presented.
- Hydrological components estimated with high temporal and spatial resolution by a novel approach based on synergistic use of Sentinel data.
- Results contribute significantly to the understanding of hydrological processes in Alpine areas and the expected effects of climate change.

Abstract

Attaining a comprehensive and reliable water balance of snow-dominated alpine catchments is fundamental for a holistic representation of the hydrological and hydrogeological processes. A major limitation to the elaboration of this balance in alpine terrain is the difficultly of data acquisition as well as the limited presence of meteorological stations. Remotely sensed data can provide valuable information for the balance elaboration at a regional scale. We exploited Sentinel-satellite data to estimate the groundwater storage for one hydrologic year in an extensive Alpine catchment located in northern Italy. Evapotranspiration (ET) and Snow Water Equivalent (SWE) were estimated once weekly with the combined use of Sentinel data, at a spatial resolution of 20 m and 30 m, respectively. Finally, the groundwater storage was estimated by means of the residual water balance approach. The results show that the adopted satellite-based methods allow obtaining consistent and physically realistic values to describe the groundwater storage dynamics, with a relatively low uncertainty (36%). For the studied hydrologic year, a positive storage occurred only in the snowmelt period and the overall storage was negative, leading to a lowering of the groundwater level in the floodplain. In addition, the influence of physiographic parameters (altitude, slope, and aspect) and the seasonal conditions on the estimates of ET and snow-depth were investigated. For SWE estimates, an altitude-dependent effect and a lower accuracy in the snowmelt phase were observed. Finally, the estimated values of ET and the SWE-linked components were verified for a gauged tributary valley with negligible groundwater storage.

1. Introduction

Understanding the storage dynamics of the groundwater resources represents one of the major contemporary challenges for water management (Bales et al., 2006; Sheffield et al., 2018; Sorg et al., 2012; Taylor et al., 2013). This is especially true for mountain areas that are recognized to be the source of much of the world's surfaces water supply (Fayad et al., 2017; Viviroli et al., 2007). In the Alpine zone, the snow-dominated catchments show a high potential of recharge due to a large precipitation and the relatively small evapotranspiration (Wilson and Guan, 2004; Hayashi, 2020). However, climate change affects surface processes such as runoff, snowpack dynamics, or evapotranspiration (Clow, 2010; Cochand et al., 2019; Rodell et al., 2018), conditioning water availability.

A major issue for alpine catchments is the heterogeneous distribution and the rapid dynamics of hydrological processes thanks to the local-scale variability of meteorological conditions and the terrain complexity. These prevent a spatial and temporal efficient input-data collection, even considering the relative scarcity of hydro-meteorological stations in such low-population areas. Accordingly, these limitations in data acquisition introduce significant approximations and uncertainty (West et al., 2019).

In the past 30 years, the advance in the ability to observe some hydrological phenomena from space has given new opportunities for their monitoring (Lettenmaier et al., 2015; McCabe et al., 2017; Tang et al., 2009) thanks to a wide variety of spatial, spectral and temporal resolutions. At watershed and regional scales, remote sensing products are deemed as a complementary source of information to in situ monitoring networks and, in many cases, the only feasible source (Sheffield et al., 2018). Except for a few studies that approached the estimation of groundwater storage in the alpine zone by using remote sensing data (Bibi et al., 2019; Gemitzi et al., 2017), most of the satellite-based methods proposed to calculate the main components of the water balance (i.e., evapotranspiration and snow water equivalent) are poorly suitable for large alpine catchments. These methods do not allow to capture topography variability, as a result of the low spatial resolution, or are still impracticable in extensive catchments (Dozer et al., 2016).

For evapotranspiration (ET), satellite data are used in several methods and models (Zhang et al., 2016). MOD16, a physical model based on the Penman-Monteith's equation, is routinely applied to generate a global ET dataset (MODIS/Terra Net Evapotranspiration 8-Day L4 Global 500 m) by using NASA MODIS (MODerate Resolution Imaging Spectroradiometer) data. This dataset provides an 8-day averaged value of ET with a spatial resolution of 500 m. Other satellite-based approaches developed in the last two decades, such as METRIC (Mapping Evapotranspiration with Internalized Calibration, Allen et al., 2007), SSEBop (Simplified Surface Energy Balance; Senay et al., 2013), ALEXI/DisALEXI (Atmosphere–Land Exchange Inverse, Anderson et al., 1997, 2007), fall into the category of the surface energy balance (SEB). In these models, ET is linked to Land Surface Temperature (LST) derived from thermal infrared (TIR) of Meteosat, MODIS and Landsat remote sensing dataset (Bhattarai et al., 2016; Castelli et al., 2018). The thermal input affects the quality and the spatial and temporal resolution of these products (Cammalleri et al., 2014). In particular, the coarse resolution does not yet completely fulfil the requirements of applications in heterogeneous areas, such as the mountain regions (Cammalleri et al., 2014; Guzinski et al., 2019; Kustas et al., 2004).

The spatial-distributed quantification of snow depth and snow water equivalent (SWE) is still problematic in mountain hydrology (Dozier et al., 2016; Liu et al., 2020). One of the most consistent methods is the spatial interpolation of local measurements of SWE, constrained by remotely sensed snow cover area (SCA) (Dozier et al., 2016). This method is physically realistic but affected by high uncertainty in the unrepresented areas and influenced by the location of the monitoring sites on flat terrain (Bavera et al., 2009; Rice et al., 2011). Another method is the backward reconstruction of the SWE accumulation time series, with a high spatial resolution (10-30m) and based on daily snowmelt and SCA changes from the last significant snowfall (Jonas et al., 2009; Liu et al., 2020). This method is still impracticable on extensive catchments for its computational load (Dozier et al., 2016). The passive microwave is at the basis of the available SWE maps (spatial resolution of 10-25km) of the northern hemisphere, such as NASA/JAXA's AMSR-E/Aqua Daily L3 Global Snow Water Equivalent EASE-Grids (AE_DySno) (Tedesco et al., 2004), NSIDC's Global EASE-Grid 8-day Blended SSM/I and MODIS Snow Cover (NSIDC-0321) (Brodzik et al., 2007). The use of the passive microwave has the advantage in the day-night all-weather capability, but it is strongly affected by the texture of the snow and the content of liquid water in the snowpack.

Recently, new opportunities for an accurate, operational, and multiply-scale estimation of the hydrological parameters are opened by Sentinel data (Guzinski et al., 2019; Veloso et al., 2017). These new freely and globally available data are collected in the Sentinel missions, launched in the last 6 years by ESA, acquiring frequent observations from a combination of optical, thermal and microwave sensors with high spatial and temporal resolutions (Guzinski et al., 2019; Malenovský et al., 2012; West et al. 2019).

The main objectives of this study are (i) to obtain a Sentinel-based methodology to quantify the seasonal groundwater storage in a snow-dominated catchment, and (ii) to apply the methodology to an extensive alpine catchment (Valtellina Valley, North Italy) for one hydrologic year (March 2018 to February 2019). For these purposes, we quantified the seasonal groundwater storage volume according to the residual water budget method (Healy et al., 2010), starting from multi-sensory Sentinel data. In particular, we tested new promising methods for the estimation of ET

(Guzinski et al., 2020) and snow depth (Lievens et al., 2019), and we investigated the inherent uncertainties. To assess the effect of physiographic characteristics (altitude, slope, and exposition) and seasonality on the storage quantification, we analysed the root mean square error (RMSE) concerning available ground truth data or to other satellite databases. Finally, we verified the ET and SWE-linked component volumes in a tributary valley, where the groundwater storage is assumed negligible.

2. Methods

2.1. Groundwater storage dynamics

The dynamics of water during the hydrologic year were investigated with the residual water-budget method (Healy et al., 2010), where all the terms of the governing equation are independently measured or estimated, and groundwater storage ($\Delta S^{gw}, [m^3/day]$) is set equal to the residual. The groundwater storage volumes were quantified for 3 different phases of the hydrologic year: (1) snowmelt; (2) snow-free; (3) snow accumulation.

For a watershed, considering snowpack (*snow*), surface water (*sw*), and water in the unsaturated (*uz*) and saturated (*gw*) zone, the water budget corresponds to the following equation:

$$\boldsymbol{P} + \boldsymbol{Q_{on}}^{\boldsymbol{sw}} + \boldsymbol{Q_{on}}^{\boldsymbol{gw}} = \boldsymbol{ET}^{\boldsymbol{sw}} + \boldsymbol{ET}^{\boldsymbol{gw}} + \boldsymbol{ET}^{\boldsymbol{uz}} + \Delta \boldsymbol{S}^{\boldsymbol{snow}} + \Delta \boldsymbol{S}^{\boldsymbol{sw}} \\ + \Delta \boldsymbol{S}^{\boldsymbol{gw}} + \Delta \boldsymbol{S}^{\boldsymbol{uz}} + \boldsymbol{Q_{off}}^{\boldsymbol{gw}} + \boldsymbol{Q_{off}}^{\boldsymbol{sw}} + \boldsymbol{Abs} \quad (1)$$

where P is the precipitation $[m^3/day]$, , Q_{on} and Q_{off} are the water flow $[m^3/day]$ into and out from surface water and groundwater systems, ET is the evapotranspiration $[m^3/day]$, ΔS is the water storage, and Abs is the anthropic abstraction $[m^3/day]$. The volume of each component was calculated considering the entire area of the catchment.

In an extensive snow-dominated catchment, the precipitation (P) and the surface-water flow into the watershed (${Q_{on}}^{sw}$), such as the snowmelt, are the two main sources of recharge during the hydrologic year. Meanwhile, the depletion of water is produced by the effect of evapotranspiration ($ET = ET^{sw} + ET^{uz} + ET^{gw}$), the storage of water in the snow-packs (ΔS^{snow}), the main river outflow from the catchment (${Q_{off}}^{sw}$) and by the abstraction (Abs). The storage of the surface-water (ΔS^{sw}) and of the unsaturated zone (ΔS^{uz}) and the flows into and out of the groundwater system (${Q_{on}}^{gw}$ and ${Q_{off}}^{gw}$) were assumed negligible given the topographical and geological setting of the catchment. Consequently, the volume of groundwater storage (ΔS^{gw}, $[m^3]$) was estimated with the water budget equation as following:

$$\Delta \boldsymbol{S}^{\boldsymbol{gw}} = (\boldsymbol{P} + \boldsymbol{Q_{on}}^{\boldsymbol{sw}}) - (\boldsymbol{ET} + \Delta \boldsymbol{S}^{\boldsymbol{snow}} + \boldsymbol{Q_{off}}^{\boldsymbol{sw}} + \boldsymbol{Abs}) \tag{2}$$

In the present work, the quantification of $Q_{off}{}^{sw}$ was carried out with the rating curves procedures at the outlet point of the catchment, the Abs from the public wells and springs data, and the daily P from PERSIANN-Cloud Classification System (PERSIANN-CCS) database (https://chrsdata.eng.uci.edu, Nguyen et al.,2019). Meanwhile, as described in the next paragraphs, $Q_{on}{}^{sw}$, ΔS^{snow} and the ET were quantified with the spatial-time-series of the ET and the SWE achieved with Sentinel-based methods. The uncertainty [%] derived from Sentinel-based data in the estimation of groundwater storage was calculated as:

$$\Delta = \sqrt{\Delta \boldsymbol{ET}^{\boldsymbol{2}} + \boldsymbol{\Delta SWE}^{\boldsymbol{2}}} \tag{3}$$

In which ΔET, [%], and ΔSWE, [%], are the values of uncertainty calculated as RMSE.

Moreover, to verify the Sentinel-based estimates of $Q_{on}{}^{sw}$, ΔS^{snow}, and ET, the $Q_{off}{}^{sw}$ of a tributary valley was achieved with equation (4), assuming a negligible ΔS^{gw}over the year and compared with the measured discharge at the outlet point:

$$\boldsymbol{Q_{off}}^{\boldsymbol{sw}} = (\boldsymbol{P} + \boldsymbol{Q_{on}}^{\boldsymbol{sw}}) - (\boldsymbol{ET} + \Delta \boldsymbol{S}^{\boldsymbol{snow}} + \boldsymbol{Abs}) \tag{4}$$

2.2.Evapotranspiration

A new method based on the synergistic use of Sentinel 2 and 3 satellite data was explored for the estimation of evapotranspiration (Guzinski et al., 2020, 2019). This method, implemented in an open-source Python library in the “Sentinels for Evapotranspiration (SEN-ET)” project (by DHI GRAS, IRTA and Sandholt ApS), aims at modelling evapotranspiration at the highest possible spatial resolution without sacrificing the output accuracy. In particular, we used the plugin of the SEN-ET algorithms (http://esa-sen4et.org/outputs/software) in the SNAP (ESA Sentinel Application Platform 7.0.0) graphical user interface (GUI). This plugin is designed to work with the products of the second level of processing for SLSTR and MSI instrument data, respectively onboard the Sentinel-3 and Sentinel-2, available for the download from the Copernicus Open Access Hub (COAH - https://scihub.copernicus.eu).

The model requires as input morphological (STRM DEM), land-use (ESA-CCI-LC 2015, available at http://maps.elie.ucl.ac.be/CCI/viewer) and meteorological (ECMWF ERA-5 dataset) data. In particular, the plugin enables to reanalyse the meteorological ERA-5 products using the DEM, to obtain the air temperature, vapour pressure, air pressure, wind speed, clear-sky incoming solar radiation, and average daily solar irradiance data.

The method involves two steps: the thermal sharpening and the land-surface energy flux model. The former allows to obtain high-resolution (20 m) Land Surface Temperature (LST) maps using a multivariate regression model with the biophysical and topographic information and exposure maps at the S3 overpass time (2020; Gao et al., 2012; Guzinski et al.,). To ensure the conservation of energy and reduce the residual bias, a bias-correction between the two thermal images with different spatial resolutions is provided within the algorithm. The land-surface energy flux model applied in this study is based on the Two-Source Energy Balance (TSEB) model (Colaizzi et al., 2012; Guzinski et al., 2020; Norman et al., 1995), which splits the surface energy fluxes between two sources, canopy and soil, derived from a measurement of the bulk surface radiometric temperature. As a result, four instantaneous land-surface energy fluxes at the time of Sentinel-3 overpass are produced by means of the Priestley-Taylor's approximation: sensible heat flux ($H, [W/m^2]$), latent heat flux ($LE, [W/m^2]$), ground heat flux ($G, [W/m^2]$) and net radiation ($R_n, [W/m^2]$):

$$\boldsymbol{R_n - G = H + LE} \tag{5}$$

Finally, the daily evapotranspiration ($ET, [mm/day]$) is extrapolated by the ratio between the instantaneous latent heat flux and daily solar irradiances $[J/m^2]$.

However, in order to evaluate the generated maps in extensive mountain areas, a comparison with two different datasets was performed. The first dataset was obtained by the meteorological stations' data applying the FAO Penman-Monteith's equation (Allen et al., 1998). The second was the MOD16A2 global evapotranspiration (MODIS/Terra Snow Cover 8-Day L3 Global 500m SIN Grid, Version 6) dataset. The correlation coefficient (r) and root mean square error (RMSE) were used to assess the goodness of fit of the satellite to the ground-based evapotranspiration estimated.

Finally, the numerical integration of the total daily evapotranspiration volume (ET_{daily}, $[m^3/day]$), calculated over the entire catchment, was used to calculate the ET for each i-th phase of the hydrologic year, as:

$$\boldsymbol{ET_i = \int_{t_0}^{t_f} ET_{daily}\, dt} \tag{6}$$

Where t_0 and t_f are the time at the beginning and at the end of the i-th phase, respectively. The uncertainty of the ET estimation (ΔET) corresponds to that of the SEN-ET method, which is reported equal to 30%, considering the root mean square error of instantaneous latent heat flux in agricultural areas (Guzinski et al., 2020).

2.3. Snow Water Equivalent

The 30-m resolution SWE maps were calculated, starting from the snow depth (SD, $[m]$) and spatially-distributed snow/water density ratio (ρ_b/ρ_w , [-]) datasets, as:

$$\boldsymbol{SWE = SD * \frac{\rho_b}{\rho_w}} \tag{7}$$

where $\rho_b, [kg/m^3]$ and $\rho_w, [kg/m^3]$ are the snow bulk density and the water density, respectively.

The SD dataset is produced by the C-Snow project (https://ees.kuleuven.be/project/c-snow), which retrieves the snowpack depth from cross-polarized backscatter measurements of the Sentinel-1 C-band (5.4 GHz, 10m) with a revisit time of 6 days. The algorithm details are presented in Lievens et al. (2019). The C-Snow dataset includes northern hemisphere maps of the snow-depth at 1km^2 spatial resolution, starting from September 2016. To improve the resolution of the snow detection, snow-cover mask for each month of the hydrologic year was applied on the SD maps. The masks were performed by processing Sentinel-2 images (20 m resolution) with cloud-free pixels classified as snow when:

$$\boldsymbol{NDSI < 0.4 \ and \ \rho_{red} < 0.2} \tag{8}$$

where NDSI is the Normalized Difference Snow Index, [-], and ρ_{red} [-] is the value of the red band (B4). The thresholds were set conservatively high to avoid false detection. Moreover, Forest Type 2015 High Resolution Layer (https://land.copernicus.eu/pan-european/high-resolution-layers) was considered to remove dense forest areas that generally could be misclassified as "no-snow".

The spatially-distributed snow density maps were achieved by applying an empirical relationship on the SRTM DEM provided by NASA JPL at a resolution of 1 arc-second (approximately 30 m at the latitude of the case study). Among the several empirical relationships to obtain ρ_b (Jonas et al., 2009; Valt et al., 2018), we adopted the linear regression equation of Bavera and De Michele (2009). This relationship considers the altitude, z $[m\,a.s.l]$, the number of days after 1st of September, D $[d]$, and the local slope, I [%], as predictors of the ρ_b:

$$\boldsymbol{\rho_b = 0.038z + 0.649D - 1.434I + 145.03 \qquad R^2 = 0.43} \tag{9}$$

To assess the validity of the method based on the use of Sentinel data, the accuracy of the SD was cross-checked with available snow gauge data. The correlation coefficient (r), and the dependence of the root mean squared error (RMSE) on physiographic parameters (altitude, slope, and aspect) and on the seasonal conditions were examined. Moreover, the uncertainty of SWE estimates, ΔSWE, was considered equal to the RMSE of snow-depth values calculated for all the available monitoring sites.

Finally, the hydrologic components linked to the snow were quantified from the time-series of the total SWE calculated at the catchment scale. As described in equation (10), the ${Q_{on}}^{sw}$, $[m^3/day]$, of each i-th phase of the hydrologic year is the sum of difference for each time step *t(i)* between the SWE, $[m^3/day]$, at time *t* and at time *t+1*, only if the difference is positive.

$$\boldsymbol{{Q_{on}}^{snow}{}_{i} = \sum_{\substack{t(i) \\ SWE_t > SWE_{t+1}}} SWE_t - SWE_{t+1}} \tag{10}$$

Conversely, the total volumes of ΔS^{snow}, $[m^3/day]$, were estimated as the positive difference between the volume of SWE at the end, t_f, and at the beginning, t_0, of the i-th phase of the hydrologic year, as:

$$\Delta \boldsymbol{S^{snow}{}_{i} = \begin{cases} 0, & SWE_{t_f} \leq SWE_{t_0} \\ SWE_{t_f} - SWE_{t_0}, & SWE_{t_f} > SWE_{t_0} \end{cases}} \tag{11}$$

3. Case study

The study was conducted in the alpine catchment of Valtellina Valley, Italy (between longitude 46° 08’00E and 46° 29’00E, and latitude 9° 31’ 00N and 10° 22’00N, Fig. 1) and in the Poschiavo tributary valley to verify the Sentinel-based estimates of the hydrological components. Valtellina valley stretches along the Adda River and covers 2,600 km^2 with a maximum relief difference of 3,000 m. Valtellina is an east–west-trending valley superimposed on the Insubric tectonic line and has a U-shaped profile derived from glacial activity. Due to a well-developed surface drainage network, several tributary valleys are located on both valley sides. The area is mostly characterised by grassland on the valley floor and broad-leaved/coniferous forest and bare rocks on the slopes. In particular, the tributary valleys, such as the Poschiavo Valley (Fig. 1), are characterized by a crystalline bedrock covered by quaternary glacial tills, fossil and recent rock glaciers, talus deposits, and large rockslides of variable thickness (De Franco et al., 2009; de Palézieux et al., 2019). Considerable glacial areas are located in three lateral valleys (Val Masino, Valmalenco and Valfurva valleys). Due to the wide range of altitude and slope aspect, a strong climatic variability and seasonal thermal contrasts characterize the area (Colombo et al., 2000). Like in other large alpine valleys, the groundwater flow in the floodplain is characterized by a relatively shallow system, in which an active circulation and a rapid response to changes in discharge and recharge are observed. Moreover, the system is highly influenced by the large hydropower production in the twenty-seven hydropower dams (from the biggest plants, such as Cancano, Alpe Gera and San Giacomo di Fraele, to the smallest ones; such as Ganda and Moledana) (D’Agata et al., 2018). For the whole catchment area, meteorological and hydrological datasets are collected continuously and made available online by the Environmental Protection Agency of Lombardia Region (ARPA-Lombardia) but some large areas, inevitably, remain unmonitored. In Table 1, the database characteristics for the present study are described. The hydrologic year considered for the application of the Sentinel-based method is March 2018 to March 2019.

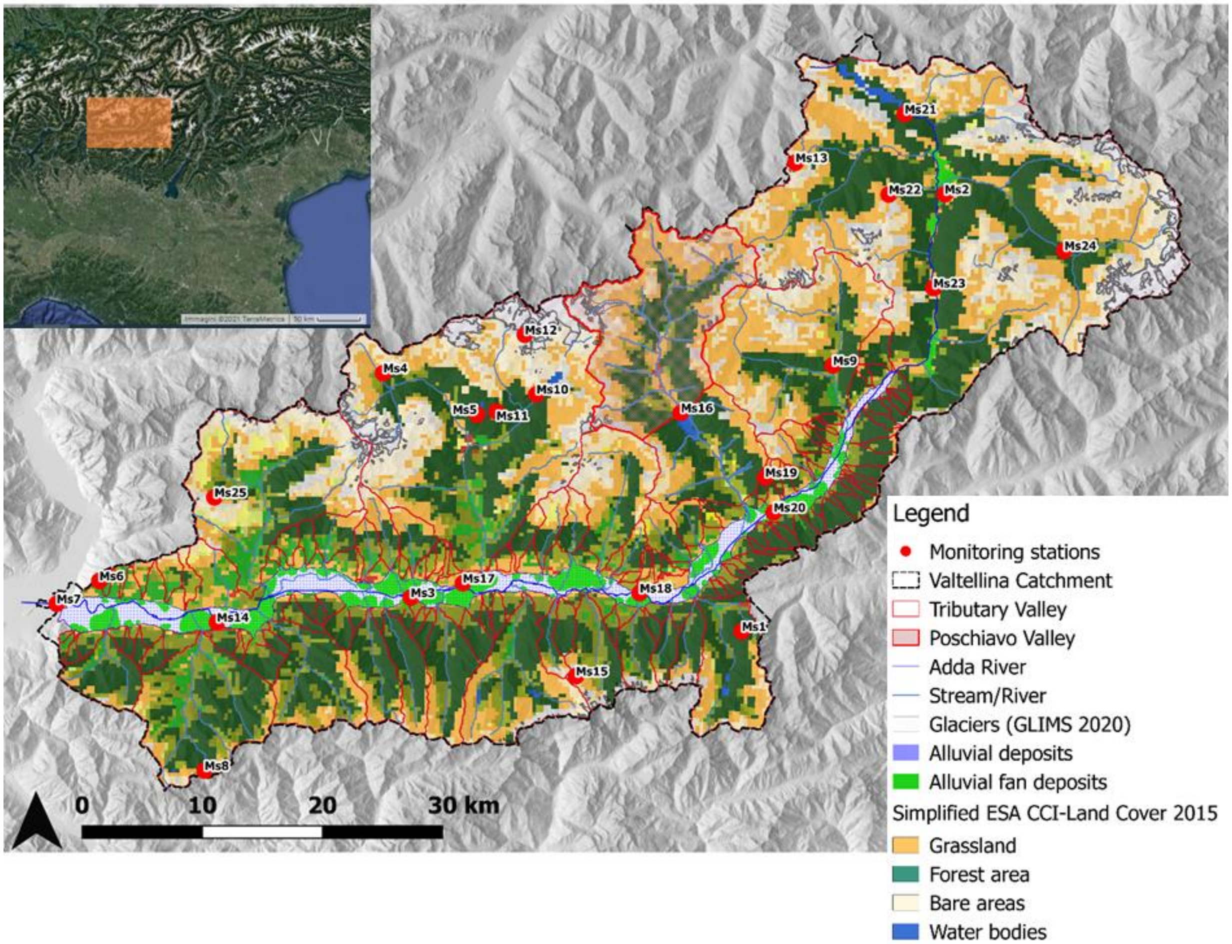

Figure 1. Map of the study area with simplified land cover and geomorphological classification and location of monitoring stations (see Table 1).

254

255

Table.1 Available monitoring stations (see Fig.1 for location) in the catchment area. T is temperature, P precipitation, SD snow depth, W is wind speed , Hum is relative humidity, R is global radiation, and Q and Hsw are discharge and stage of the stream.

	STATION	ALT [m a.s.l.]	LAT WGS84 [DD]	LON WGS84 [DD]	VARIABLE	RESOLUTION USED	TIME INTERVAL
MS01	Aprica	1950	46.129688	10.148266	SD, P	Daily	2016-2020
MS02	BORMIO eliporto	1172	46.453701	10.366032	P, T	Daily	2016-2020
MS03	CAIOLO	274	46.154927	9.792523	P, T, W, Hum, R	Daily	2016-2020
MS04	CHIESA IN VALMALENCO Alpe dell'Oro	2040	46.321466	9.763076	SD, P	Daily	2016-2020
MS05	CHIESA IN VALMALENCO Funivia Bernina	2014	46.290759	9.863706	SD, P	Daily	2016-2020
MS06	DUBINO La Piazza	993	46.167263	9.458140	P	Daily	2016-2020
MS07	GERA LARIO - Fuentes	199	46.150329	9.412275	P, T, Q	Daily	2016-2020
MS08	GEROLA ALTA Pescegallo	1875	46.026197	9.571121	SD, P	Daily	2016-2020
MS09	GROSIO Diga Fusino	1220	46.327062	10.245981	SD, P	Daily	2016-2020
MS10	LANZADA Campo Moro	1970	46.305757	9.927520	SD, P	Daily	2016-2020
MS11	LANZADA Palù	2151	46.292907	9.884528	SD, P	Daily	2016-2020
MS12	LANZADA Passo Marinelli	3032	46.349810	9.915154	SD, P	Daily	2016-2020
MS13	LIVIGNO - La Vallaccia	2660	46.477098	10.205837	SD, P	Daily	2016-2020
MS14	MORBEGNO eliporto	230	46.136635	9.584344	P, T, W, Hum, R	Daily	2016-2020
MS15	PONTE IN VALTELLINA Lago Reguzzo	2440	46.096514	9.969999	SD, P	Daily	2016-2020
MS16	POSCHIAVO	959	46.291989	10.082806	Hsw-Q	Daily	2018-2019
MS17	SONDRIO Fond.Fojanini	307	46.165595	9.848505	P, T, W, Hum, R	Daily	2016-2020
MS18	TEGLIO S. Giacomo	357	46.158277	10.038480	P, Hsw-Q	Daily	2016-2020
MS19	TIRANO Monte Masuccio	1750	46.244091	10.173320	SD	Daily	2016-2020
MS20	TIRANO eliporto	481	46.218168	10.182292	P, T, W, Hum, R	Daily	2018-2020
MS21	VALDIDENTRO - Cancano	1948	46.512933	10.323059	SD, P	Daily	2016-2020
MS22	VALDISOTTO Oga S. Colombano	2300	46.453565	10.305964	SD, P	Daily	2016-2020
MS23	VALDISOTTO Arginone	1050	46.384385	10.353989	SD, P	Daily	2016-2020
MS24	VALFURVA S. Caterina	1730	46.412150	10.494665	SD, P	Daily	2016-2020
MS25	VAL MASINO S.Martino	1950	46.229316	9.581636	SD, P	Daily	2016-2020

4. Analysis and Results

4.1. Evapotranspiration estimation

Spatial distribution of evapotranspiration was produced for the 2018-2019 hydrologic year with a monthly average of 8 maps using:

- 34 Sentinel-2A and Sentinel-2B MSIL2A images, selected from the T32TNS and T32TPS tiles with a maximum cloud cover percentage of 20%. The downloaded data of the two tiles were extracted in the area of interest and merged into 17 images.

- 163 Sentinel-3A SL_2_LST images with sensing data in the morning. After the extraction into the area of interest, 109 images were selected by considering cloud cover percentage.

During the first part of the hydrologic year, the results show an ET increase from March to the 15 June, with a mean of 4.0±1.0 mm/day for the grassland and of 3.9±1.3 mm/day for the forest cover (Fig. 2a). An anomalous spike of evapotranspiration is observed at the end of April (Fig. 3). The maximum ET value is recognized at the beginning of the snow-free phase, with the peak recorded on the 18 July with a mean value of 5.2±0.9 mm/day for the grassland and of 5.8±0.7 mm/day for the forest cover (Fig. 2b). Successively, the ET shows a strong decrease until the end of October, with a minimum value equal to 1.5±0.5 mm/day in the grassland and of 1.8±0.4 mm/day in the forest area (Fig. 2c). At the end of the hydrologic year, the results show a constant minimum value of ET (≈0.01 mm/day) with a slight increment in February. Due to the snow accumulation and the decrease in average temperature, the ET is equal to 0 mm/day over an increasingly higher percentage (max≈17%) of the area. Anyway, at the end of February (Fig. 2d), the ET average stands at 1.5±0.8 mm/day and of 1.1±0.8 mm/day for the grassland and the forest cover, respectively.

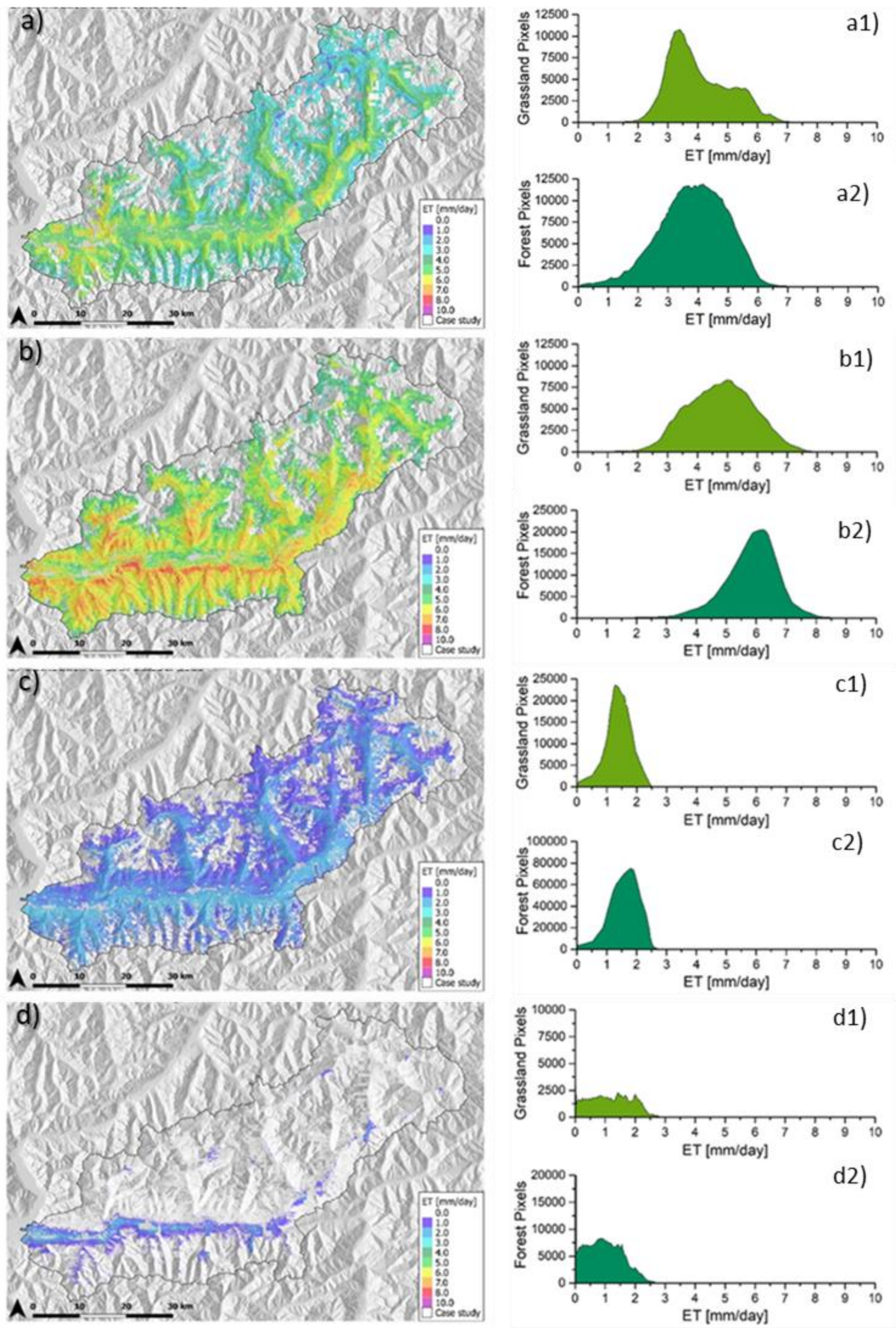

Figure 2 Maps of daily evapotranspiration (ET) during four representative days in different seasons of the 2018-2019 hydrologic year and corresponding evapotranspiration frequency distributions in grassland and forest areas. a) 15 June 2018; b) 18 July 2018; c) 19 October 2018; d) 21 February, 2019.

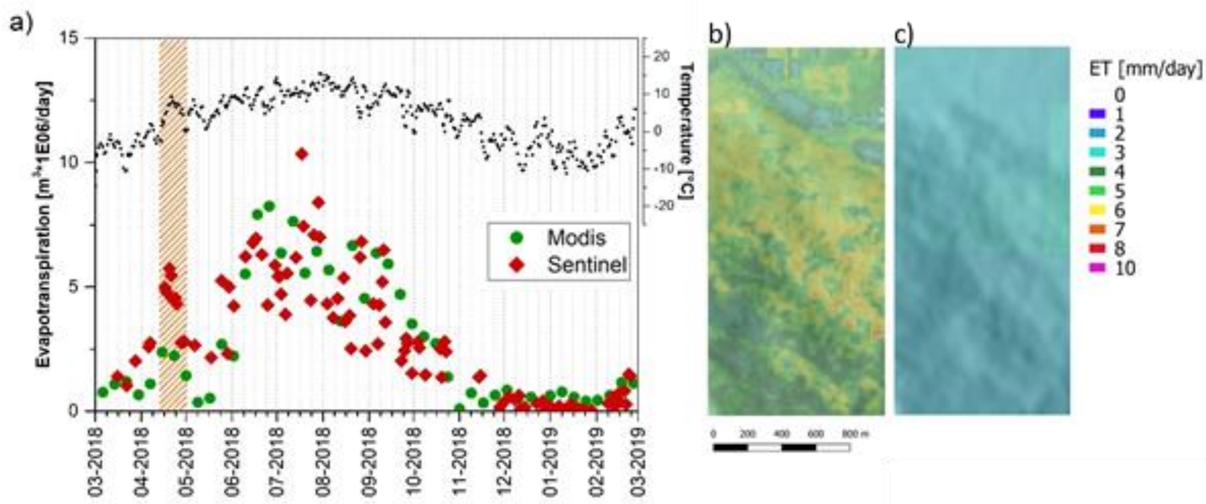

Figure 3 a) Time series of daily evapotranspiration volumes estimated at the basin scale with Sentinel data (red diamonds) and MODIS (green circles) data. b) and c) maps of daily ET spatial distribution on 20 April 2018 with Sentinel (b) and MODIS (c) data, showing the capability of Sentinel to recognize the temperature anomaly of April.

The comparison among the ET values estimated with the Sentinel and Modis data and the ground data at 4 locations is shown in Fig. 4. The results indicate a significant correlation ($p<0.05$) with the ground-based ET for both the MOD16A2 ($r=0.72$, RMSE=0.82 mm) and the Sentinel products ($r=0.72$, RMSE=1.0 mm). However, the Sentinel product provides a better fitting with ground data during the snowmelt phase.

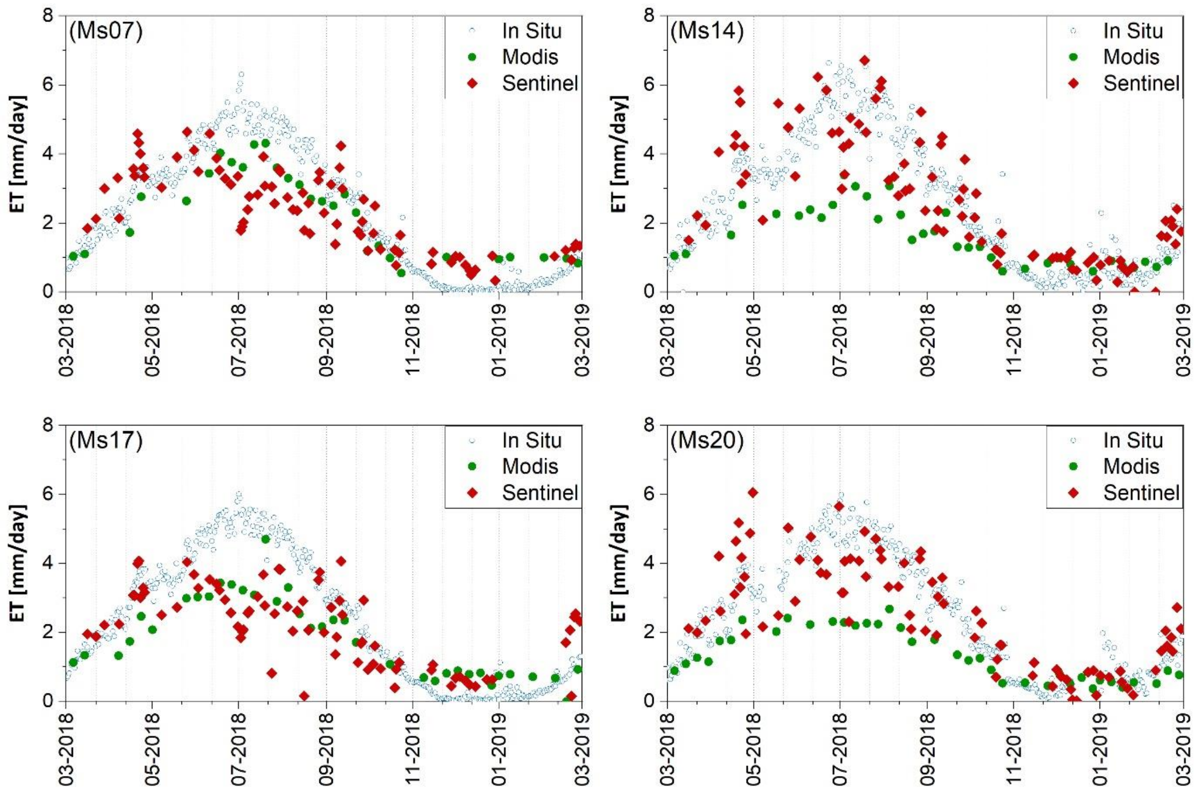

Figure 4 Comparison among the ET time series for the 2018-2019's hydrologic year, estimated with the Sentinel and Modis data and the ground data at the monitoring stations Ms07, Ms14, Ms17 and Ms20 (see Fig.1).

At the catchment scale, the comparison between the two different satellite data products shows a comparable total volume of evapotranspiration during the hydrological year (9.3x1E8 m^3/year vs 9.1X1E8 m^3/year), considering the uncertainty (ΔET) of the 30%.

4.2.Snow water equivalent estimation

The SWE product for the 2018-2019 hydrologic year consists of 113 maps at the resolution of 30 m. For the spatial constrain, the monthly S2-based snow cover area was considered. Figure 5 shows the distribution of the snow water equivalent during the hydrologic year. At the starting point of the snowmelt phase (Fig.5a), the snow line is located between 1,800 m a.s.l. and 2,300 m a.s.l and the maximum height of the snow equivalent is estimated equal to 2.00 m at high altitude. The total volume of water stored in the snow was estimated equal to 4.7E8 m^3. The retrieves of the snow depth confirm a snow-free phase between July and September, in line with historical trends (Bavera et al 2009). The first evidence of snow is observed after the first snowfall event at the end of October (Fig.5b), storing 1.1E+08 m^3 of water. The accumulation of the snow increases until February when the snow line reaches the altitude of 1,800 m a.s.l., and the low-altitude slopes exposed to the north locally. At the end of the hydrologic year (Fig.5c) the maximum snow water equivalent was 2.0 m at high altitude, and the total water volumes stored was 7.65E+08 m^3.

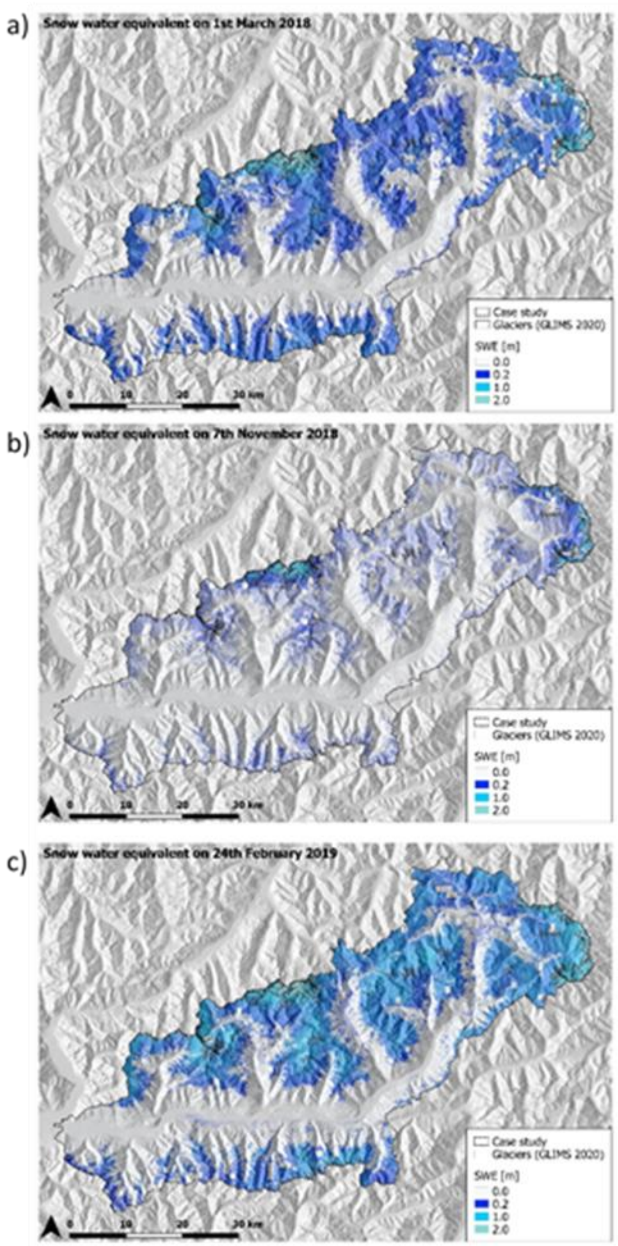

Figure 5 Maps of daily snow water equivalent (SWE) for three representative days in different seasons of the 2018-2019 hydrologic year. a) 1 March 2018; b) 7 November 2018; c) 24 February 2019.

The uncertainty and the variability of the RMSE of the results, for the aim of this research, is linked only to the SD and not to the density. The snow-density distribution, empirically obtained (Bavera et al., 2009) on the SRTM DEM at 30m of resolution, has an average of 240±30 kg/m³ during the snow accumulation phase, and an average of 350±30 kg/m³, with a maximum value of 460 kg/m³ at high altitude, in the snowmelt phase. For the validation of the C-snow database (from 2016 to 2020), the data from 16 snow gauge stations were available in the catchment, covering different altitude zones (Tab 1). The average weekly snow depth (m) at the measurement sites and corresponding Sentinel-1 grid cells were compared. The uncertainty (ΔSWE), considering the total time series, amounts to 20%. The reliability is proved by a significant temporal correlation (r=0.66, p<0.05) and a RMSE of 0.57m (Tab.2), although the trend of the residuals (Fig. 6a) during the year underestimate the snow depth in the snowmelt phase. Moreover, considering the four winter seasons available, the higher average RMSE at the gauge stations was recorded for the 2018-2019's year (Fig. 6b). Figures 6c-e show the analysis of the dependence of the RMSE on the spatial location. It is worth remarking that, to exposure and slope, altitude influences more the difference between the Sentinel and in-situ data, with an increase in RMSE of ca. 0.02 m every 100 m and that, in the proximity of the snow line, the correlation is reduced.

Table.2 Statistical relations between measured and retrieved snow depths for the total time series and for the time series of the season available.

SERIES	PEARSON'S R	RMSE [m]	NRMSE [-]
TS_TOTAL	0.66 (<0.01)	0.57	0.20
TS_2016-2017	0.47 (<0.01)	0.45	0.19
TS_2017-2018	0.51 (<0.01)	0.62	0.23
TS_2018-2019	0.76 (<0.01)	0.66	0.19
TS_2019-2020	0.76 (<0.01)	0.53	0.18

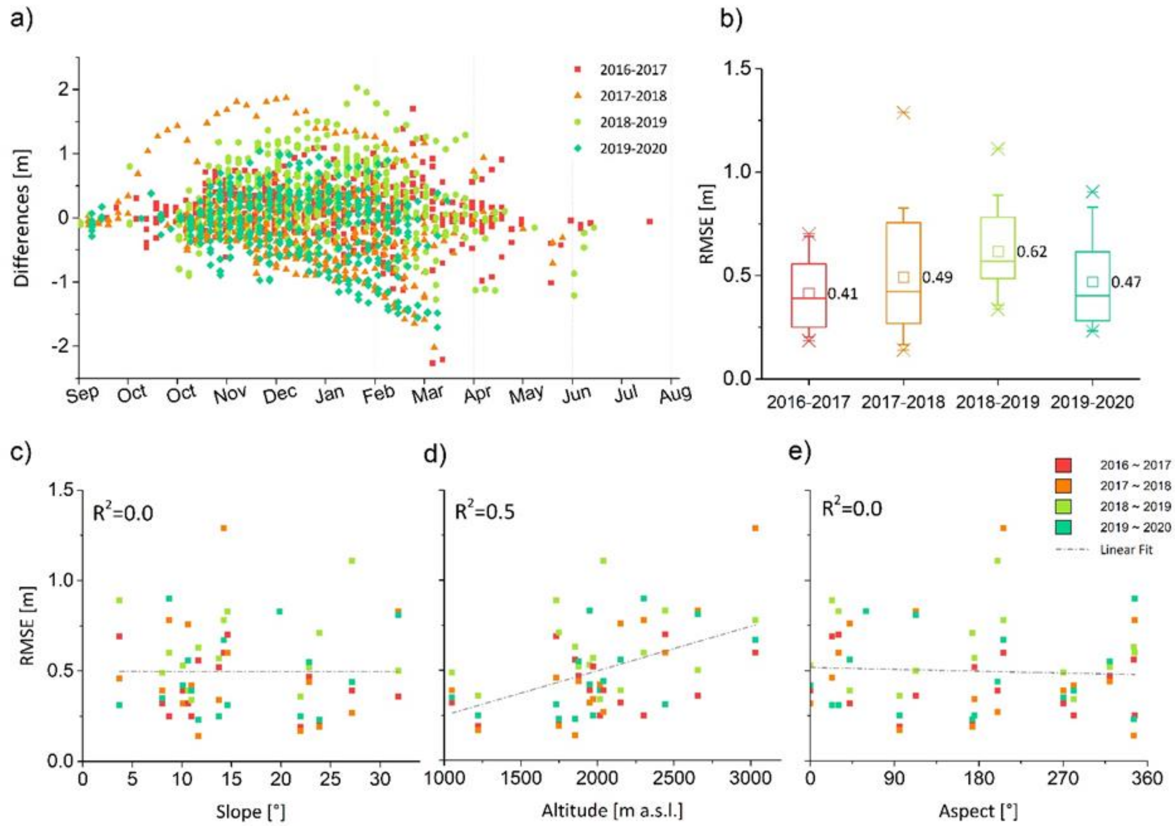

Figure 6 Comparison between C-SNOW and ground-monitored weekly snow-depth values at monitoring stations (Tab 1). a) Temporal pattern of the difference between snow-depth values during four hydrologic years. b) RMSE of snow-depth values. c, d, and e) relationship of RMSE of snow-depth values with: c) slope gradient (RMSE = 0.50 -5.6e-5 Slope, R^2 = 0.0); d), altitude (RMSE =2.5e-4 Altitude, R^2 = 0.5); and e) slope aspect (RMSE = 0.52-1.1E-4 Aspect, R^2 = 0.0)

4.3.Quantification of groundwater storage dynamics

The dynamics of storage was achieved by quantifying the volumes involved in each hydrologic process during the 3 phases of the 2018-2019 hydrologic year in the Valtellina valley. The overall uncertainty (Δ) of the Sentinel-based method amounts to about 36%, due to the uncertainty of ET (30%) and SWE (20%).

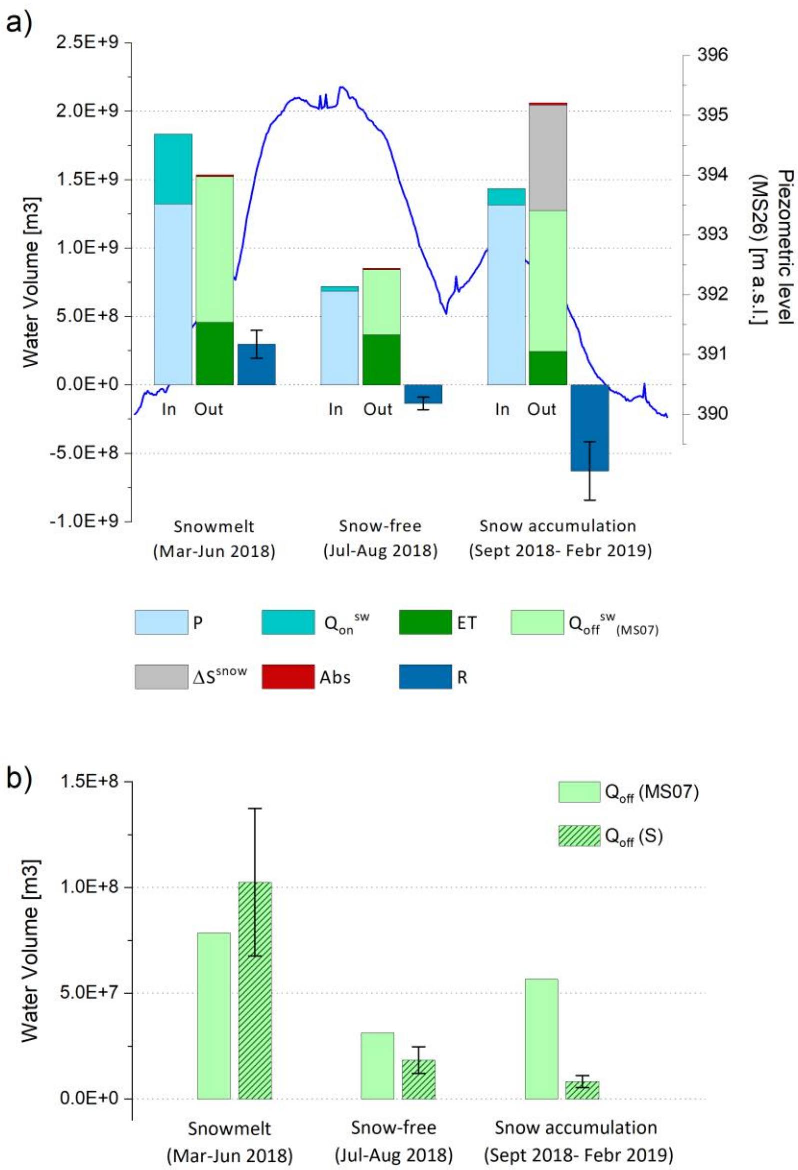

Figure 7 a) Water balance for different periods of the year (snowmelt period, snow-free period, and snow accumulation period) between the 01 March 2018 and 28 February 2019. Error bars represent the uncertainty associated to the use of Sentinel-based method for the estimation of the groundwater storage. In the background, the fluctuations of the groundwater level measured in the floodplain during the year. b) Comparison of the volumes of water output to the MS16 obtained with the method based on sentinel data and with the data in situ, for the valley of Poschiavo (in red in the map). Error bars represent the uncertainty associated to the use of Sentinel-based method for the prediction of discharge. P = Persian-based precipitation; ${Q_{on}}^{sw}$ = Sentinel-based snowmelt; ET^{sw}= Sentinel-based Evapotranspiration; ${Q_{off}}^{sw}$ = measured discharge; ΔS^{snow}= Sentinel-based stored snow; Abs = measured anthropic abstraction; ΔS^{gw} = Sentinel-based groundwater storage; $Q_{off}(S)$= Sentinel-based discharge.

At the catchment scale, the residual water-budget (Fig.7a) was achieved considering the Ms07 (Fig.1) as outlet point. During the first phase (March to June), the groundwater storage reaches the peak value, with an average of 1.3±0.4 mm/day, mainly due to the effect of precipitation and snowmelt. During the snow-free phase (July to September), we observe the first part of the recession curve in which the catchment outflow is larger than the total precipitation. The loss of water amounts to about 45% of the antecedent-phase recharge. The decrease is due almost equally to the evapotranspiration (43.5% of the output) and the runoff (56.5% of the output) related to heavy and instantaneous rainfall events. In the snow accumulation phase (October to February), additional depletion of the storage (1.3±0.4 mm/day) is observed as a result of the surface flow (50.4% of the output) and the storage of water as snow (37.6% of the output), despite the instantaneous peaks of recharge due to the heavy rainfall events.

For the Poschiavo valley, the estimated surface-flow in the main river, Poschiavino River, was compared with the discharge data at the Ms16 (Fig. 7b). For the whole year, the volume of ${Q_{off}}^{sw}$ corresponds well to the measured discharge, with a difference of 27.4%. Considering the three phases, we observe that the measured discharges lie within the uncertainty range of the estimated ${Q_{off}}^{sw}$, except for the snow-accumulation phase. In this phase, the Sentinel-based ${Q_{off}}^{sw}$ significantly underestimate the measured discharge.

5. Discussion

5.1. Water dynamics

The application of Sentinel-based methods for the analysis of the groundwater recharge and storage provides consistent and physically realistic values for extensive alpine catchments. This is demonstrated by an uncertainty (Δ =36%) relatively small, considering other remote sensing methods (Dozier et al., 2016; Karimi et al., 2015). Although limited to a single hydrologic year, the results allow obtaining a preliminary understanding of the storage dynamics in the Alpine area. First of all, a positive groundwater storage is limited only to the snowmelt phase. In the rest of the year, the storage is negative, also during the snow accumulation phase when the precipitation input is significant but stored in the snowpack. However, the negative values for 2018 may be overestimated due to the high RMSE in the estimation of snow depth in the 2018-2019 winter (Tab. 2). Morover, it is important to note that an underestimation of the balance could be due to the assumption that some components, such as the ${Q_{on}}^{gw}$, are neglected. In any case, a negative overall annual storage is confirmed by the groundwater levels measured along the main floodplain of the catchment, where the piezometers show a net annual lowering of about 0.10 m.

Previous studies have shown similar dynamics in snow-dominated areas. Based on to the Special Report on Emission Scenarios (SRES), Eckhardt and Ulbrich (2003) and Neukum and Azzam (2012) found that climate change could increase groundwater recharge in spring and winter, partially associated to lower river discharge, and decrease recharge during summer and autumn, with higher river discharge. Likewise, in well-constrained water balance studies by Hood and Hayashi (2015) and Cochand et al. (2019) the groundwater storage in alpine catchments shown an excess volume of water recharge during the melting period, and an excess volume output in the late season, with an overall negative yearly storage.

The reliability of Sentinel-based estimations of the ET and the SWE-linked components has been verified with the ${Q_{off}}^{sw}$ quantification in the Poschiavo tributary valley, where the groundwater storage is assumed to be negligible. The observed discrepancies in the discharge volumes are due to the management of the 7 hydropower plants located in the Poschiavo valley. In fact, part of the water is stored during the spring season, leading to an overestimation of ${Q_{off}}^{sw}$ with respect to the measured discharge, and released in winter, leading to an underestimation (Fig. 7b).

5.2.Comparison of ET and SWE products

The Sentinel-based values of ET and SWE show a good correlation with ground measurements, supporting the use of these new remote sensing based methods to compensate for the lack of ground data. In particular, the high resolution that we were able to achieve with the Sentinel data enabled us to catch the complexity of the physiographic elements in mountain areas, as demonstrated, for instance, by the wide variability of ET values calculated along the slopes (Fig.3). Moreover, for the ET, in agreement with the results previously reported by Guzinski et al (2019), a good correspondence with the ground-based estimations of evapotranspiration was observed (Fig.4), considering the uncertainty related to the quality of the LST maps. However, since the meteorological stations for the ET computation are available only in the floodplain, it was not possible to investigate the dependence of the elevation and the exposure in the application of SEN-ET algorithm. Regarding the snow depth, an altitude-dependent discrepancy with the in-situ gauge station values is detected (Fig. 6d). It is important to remark that the meteorological monitoring sites in the mountains, especially at high altitude, lie usually on nearly flat terrain for logistical reasons. Therefore, they may not fully represent snow accumulation and melt rates on nearby slopes and in the entire pixel areas in which the stations are located (Dozier et al 2016).

This research shows that the methodology for ET estimation offers time series that may be useful for climate change analysis, since they are capable to highlight anomalies and variations. For instance, it is important to highlight the effect of the air temperature anomaly of April 2018, associated with a recorded temperature 3-5°C higher than the seasonal average (https://www.ncdc.noaa.gov/temp-and-precip/global-maps). The anomaly in the whole catchment area is clearly shown in the Sentinel-based estimation (Fig. 3), in which the values of ET result twice those expected considering the seasonal trend. The integration of the surface temperature enables to catch the seasonal fluctuations, in contrast to other methods such as in the MOD16 algorithm.

5.3.Spatio-temporal resolution

Sentinel-based methods offer maps with the highest spatio-temporal resolution currently available to estimate ET and SWE for extensive study areas. The temporal resolution is controlled by satellite overpass and clear-sky/seasonal conditions. In large mountain catchments, the size of the area reduces the availability of useful satellite images. The full spatial coverage of the area is not guaranteed at each overpass of the satellite, offering at times incomplete information for catchment-scale studies. Moreover, at high-altitude, satellite imagery is frequently affected by cirrus clouds with an occurrence larger than 50% over the mid-latitude area (Schläpfer et al., 2020). For instance, this limitation causes information gaps during the rainy months of May and November 2018, when only three maps per month are available for the ET estimation. In addition, the C-SNOW dataset shows a temporal gap during the snowmelt phase, as conveyed by Lievens et al. (2019). In fact, due to wet-snow conditions that partially reflect and absorb the radar signal, the snow-depth retrieved by Sentinel-1 is affected by a higher uncertainty. Even considering all the above limitations, the Sentinel-based methods provided a substantial coverage for about 33% of the days of the year.

Regarding the spatial resolution, the methodology allowed us to obtain a resolution of 20 m for ET and 30 m for SWE. The 20 m resolution of Sentinel-based ET is due to the sharpening of the original Sentinel-3 imagery. Higher-resolution thermal remote sensing data that are expected to be available in the future will further improve energy flux models based on satellite data in complex terrain (Castelli et al 2018). For the SWE, the resolution derives from the SRTM matched with 1 km snow depth maps. The resolution of C-SNOW SD induces higher uncertainty in the transition zones. The application of the Sentinel-2 SCA enables to reduce the uncertainty at the boundaries, close to the snow line. However, the results may further improve by taking advantage of the Sentinel-1 full resolution (about 10 m), already planned in the next implementation for the snow depth retrieves (Lievens et al., 2019).

6. Conclusions

We propose a Sentinel-based methodology to quantify the seasonal groundwater storage in a snow-dominated catchment. It consists of the application of new promising method for the estimation of ET (Guzinski et al., 2020) and the new database of snow depth (Lievens et al., 2019) in the residual water balance approach. The use of Sentinel data provides estimates of ET and SWE with a weekly frequency and a remarkable spatial resolution of 20 m for ET and 30 m for SWE. Applied to an extensive alpine catchment, this spatial and temporal resolution allows obtaining consistent and physically realistic values for extensive alpine catchments, as demonstrated by a relatively limited uncertainty (Δ =36%). Through the test of the reliability of the discharge volumes in a gauged tributary valley with negligible groundwater storage, a secondary application of the Sentinel-based ET and SWE-linked components was found, defining the runoff volumes at the outlet point in the three phases of the hydrologic year. The high temporal and spatial resolution enables to investigate the influence of physiographic parameters (altitude, slope, and aspect) and the seasonal conditions in the ET and SWE estimates. The overall negative storage for the 2018-2019 hydrological year shows a reduced high recharge potential related to high precipitation and low evapotranspiration, highlighting the possible effects of climate change on the hydrological processes and to manage the water resources in alpine snow-dominated catchments.

To the authors' best knowledge, this is the first time the groundwater storage was estimated in an extensive alpine catchment based on the synergistic use of satellite data. Moreover, the free-availability of the Sentinel data and of the algorithms for the estimation of the ET and SWE components ensure a methodology that can be applied to other catchments. The high spatial and temporal resolution of the obtained groundwater storage estimates allow to significantly contribute to the understanding of hydrogeological processes in Alpine areas, opening new frontiers to improve the elaboration and calibration of a numerical model.

Acknowledgments, Samples, and Data

The authors would like to thank Roberto Colombo and Marco Celesti from UNIMIB for their supporting in the remote sensing data management. The authors are grateful to Valeria Marchese, Zocchia Cristina, and Cipriano Giuseppa (ARPA-Lombardia) for providing meteorological and hydrological datasets. The autors declare no conflicts of interests. C-snow datasets for this research is available in these in-text data citation references: Lievens et al. (2019).

References

Allen, R. G., Pereira, L. S., Raes, D., & Smith, M. (1998). FAO Irrigation and drainage paper No. 56. Rome: *Food and Agriculture Organization of the United Nations*, 56(97), e156.

Allen, R. G., Tasumi, M., & Trezza, R. (2007). Satellite-based energy balance for mapping evapotranspiration with internalized calibration (METRIC)—Model. *Journal of irrigation and drainage engineering*, 133(4), 380-394.

Anderson, M. C., Kustas, W. P., & Norman, J. M. (2007). Upscaling flux observations from local to continental scales using thermal remote sensing. *Agronomy Journal*, 99(1), 240-254.

Anderson, M. C., Norman, J. M., Diak, G. R., Kustas, W. P., & Mecikalski, J. R. (1997). A two-source time-integrated model for estimating surface fluxes using thermal infrared remote sensing. *Remote sensing of environment*, 60(2), 195-216..

Bales, R. C., Molotch, N. P., Painter, T. H., Dettinger, M. D., Rice, R., & Dozier, J. (2006). Mountain hydrology of the western United States. *Water Resources Research*, 42(8).

Bavera, D., & De Michele, C. (2009). Snow water equivalent estimation in the Mallero basin using snow gauge data and MODIS images and fieldwork validation. *Hydrological Processes: An International Journal*, 23(14), 1961-1972.

Bhattarai, N., Shaw, S. B., Quackenbush, L. J., Im, J., & Niraula, R. (2016). Evaluating five remote sensing based single-source surface energy balance models for estimating daily evapotranspiration in a humid subtropical climate. *International journal of applied earth observation and geoinformation*, 49, 75-86.

Bibi, S., Wang, L., Li, X., Zhang, X., & Chen, D. (2019). Response of groundwater storage and recharge in the Qaidam Basin (Tibetan Plateau) to climate variations from 2002 to 2016. *Journal of Geophysical Research: Atmospheres*, 124(17-18), 9918-9934.

Brodzik, M. J., Armstrong, R., & Savoie, M. (2007). Global EASE-grid 8-day blended SSM/I and MODIS snow cover. National Snow and Ice Data Center, Boulder, CO, digital media. [Available online at http://nsidc. org/data/nsidc-0321. html.].

Cammalleri, C., Anderson, M. C., Gao, F., Hain, C. R., & Kustas, W. P. (2014). Mapping daily evapotranspiration at field scales over rainfed and irrigated agricultural areas using remote sensing data fusion. *Agricultural and forest meteorology*, 186, 1-11.

Cartwright, I., Morgenstern, U., Hofmann, H., & Gilfedder, B. (2020). Comparisons and uncertainties of recharge estimates in a temperate alpine catchment. *Journal of Hydrology*, 590, 125558.

Castelli, M., Anderson, M. C., Yang, Y., Wohlfahrt, G., Bertoldi, G., Niedrist, G., & Notarnicola, C. (2018). Two-source energy balance modeling of evapotranspiration in Alpine grasslands. *Remote Sensing of Environment*, 209, 327-342.

Clow, D. W. (2010). Changes in the timing of snowmelt and streamflow in Colorado: a response to recent warming. *Journal of Climate*, 23(9), 2293-2306.

Colaizzi, P. D., Kustas, W. P., Anderson, M. C., Agam, N., Tolk, J. A., Evett, S. R., & O'Shaughnessy, S. A. (2012). Two-source energy balance model estimates of evapotranspiration using component and composite surface temperatures. *Advances in water resources*, 50, 134-151.

Colombo, M., (2000). Inquadramento climatico statico e dinamico. [Online]Available at: http://www.aineva.it/pubblica/neve43/colombo3.htm

Dassargues, A. (2018). Hydrogeology: groundwater science and engineering. *CRC Press*.

D'Agata, C., Bocchiola, D., Soncini, A., Maragno, D., Smiraglia, C., & Diolaiuti, G. A. (2018). Recent area and volume loss of Alpine glaciers in the Adda River of Italy and their contribution to hydropower production. *Cold Regions Science and Technology*, 148, 172-184.

De Franco, R., Biella, G., Caielli, G., Berra, F., Guglielmin, M., Lozej, A., & Sciunnach, D. (2009). Overview of high-resolution seismic prospecting in pre-Alpine and Alpine basins. *Quaternary International*, 204(1-2), 65-75.

De Palézieux, L., & Loew, S. (2019). Long-term transient groundwater pressure and deep infiltration in Alpine mountain slopes (Poschiavo Valley, Switzerland*). Hydrogeology Journal*, 27(8), 2817-2834.

Dozier, J., Bair, E. H., & Davis, R. E. (2016). Estimating the spatial distribution of snow water equivalent in the world's mountains. *Wiley Interdisciplinary Reviews: Water*, 3(3), 461-474.

Eckhardt, K., & Ulbrich, U. (2003). Potential impacts of climate change on groundwater recharge and streamflow in a central European low mountain range. *Journal of Hydrology*, 284(1-4), 244-252.

Fayad, A., Gascoin, S., Faour, G., López-Moreno, J. I., Drapeau, L., Le Page, M., & Escadafal, R. (2017). Snow hydrology in Mediterranean mountain regions: A review. *Journal of Hydrology*, 551, 374-396.

Gao, F., Kustas, W. P., & Anderson, M. C. (2012). A data mining approach for sharpening thermal satellite imagery over land. *Remote Sensing*, 4(11), 3287-3319.

Gemitzi, A., Ajami, H., & Richnow, H. H. (2017). Developing empirical monthly groundwater recharge equations based on modeling and remote sensing data–Modeling future groundwater recharge to predict potential climate change impacts. *Journal of hydrology*, 546, 1-13.

Guzinski, R., & Nieto, H. (2019). Evaluating the feasibility of using Sentinel-2 and Sentinel-3 satellites for high-resolution evapotranspiration estimations. *Remote Sensing of Environment*, 221, 157-172.

Guzinski, R., Nieto, H., Sandholt, I., & Karamitilios, G. (2020). Modelling High-Resolution Actual Evapotranspiration through Sentinel-2 and Sentinel-3 Data Fusion. *Remote Sensing*, 12(9), 1433.

Hayashi, M. (2020). Alpine hydrogeology: The critical role of groundwater in sourcing the headwaters of the world. *Groundwater*, 58(4), 498-510.

Healy, R. W. (2010). Estimating groundwater recharge. Cambridge University Press.

Jonas, T., Marty, C., & Magnusson, J. (2009). Estimating the snow water equivalent from snow depth measurements in the Swiss Alps. *Journal of Hydrology*, 378(1-2), 161-167.

Karimi, P., & Bastiaanssen, W. G. (2015). Spatial evapotranspiration, rainfall and land use data in water accounting–Part 1: Review of the accuracy of the remote sensing data. *Hydrology and Earth System Sciences*, 19(1), 507-532.

Kustas, W. P., Li, F., Jackson, T. J., Prueger, J. H., MacPherson, J. I., & Wolde, M. (2004). Effects of remote sensing pixel resolution on modeled energy flux variability of croplands in Iowa. *Remote sensing of Environment*, 92(4), 535-547.

Lettenmaier, D. P., Alsdorf, D., Dozier, J., Huffman, G. J., Pan, M., & Wood, E. F. (2015). Inroads of remote sensing into hydrologic science during the WRR era. *Water Resources Research*, 51(9), 7309-7342.

Lievens, H., Demuzere, M., Marshall, H. P., Reichle, R. H., Brucker, L., Brangers, I., & Jonas, T. (2019). Snow depth variability in the Northern Hemisphere mountains observed from space. *Nature communications*, 10(1), 1-12.

Liu, M., Xiong, C., Pan, J., Wang, T., Shi, J., & Wang, N. (2020). High-Resolution Reconstruction of the Maximum Snow Water Equivalent Based on Remote Sensing Data in a Mountainous Area. *Remote Sensing*, 12(3), 460.

Malenovský, Z., Rott, H., Cihlar, J., Schaepman, M. E., García-Santos, G., Fernandes, R., & Berger, M. (2012). Sentinels for science: Potential of Sentinel-1,-2, and-3 missions for scientific observations of ocean, cryosphere, and land. *Remote Sensing of environment*, 120, 91-101.

McCabe, M. F., Rodell, M., Alsdorf, D. E., Miralles, D. G., Uijlenhoet, R., Wagner, W., & Shi, J. (2017). The future of Earth observation in hydrology. *Hydrology and earth system sciences*, 21(7), 3879.

Neukum, C., & Azzam, R. (2012). Impact of climate change on groundwater recharge in a small catchment in the Black Forest, Germany. *Hydrogeology Journal*, 20(3), 547-560.

Nguyen, P., Shearer, E. J., Tran, H., Ombadi, M., Hayatbini, N., Palacios, T., & Kuligowski, B. (2019). The CHRS Data Portal, an easily accessible public repository for PERSIANN global satellite precipitation data. *Scientific data*, 6(1), 1-10.

Norman, J. M., Kustas, W. P., & Humes, K. S. (1995). Source approach for estimating soil and vegetation energy fluxes in observations of directional radiometric surface temperature. *Agricultural and Forest Meteorology*, 77(3-4), 263-293.

Rice, R., Bales, R. C., Painter, T. H., & Dozier, J. (2011). Snow water equivalent along elevation gradients in the Merced and Tuolumne River basins of the Sierra Nevada. *Water Resources Research*, 47(8).

Rodell, M., Famiglietti, J. S., Wiese, D. N., Reager, J. T., Beaudoing, H. K., Landerer, F. W., & Lo, M. H. (2018). Emerging trends in global freshwater availability. *Nature*, 557(7707), 651-659.

Schläpfer, D., Richter, R., & Reinartz, P. (2020). Elevation-Dependent Removal of Cirrus Clouds in Satellite Imagery. *Remote Sensing*, 12(3), 494.

Senay, G. B., Bohms, S., Singh, R. K., Gowda, P. H., Velpuri, N. M., Alemu, H., & Verdin, J. P. (2013). Operational evapotranspiration mapping using remote sensing and weather datasets: A new parameterization for the SSEB approach. *JAWRA Journal of the American Water Resources Association*, 49(3), 577-591.

Sheffield, J., Wood, E. F., Pan, M., Beck, H., Coccia, G., Serrat-Capdevila, A., & Verbist, K. (2018). Satellite remote sensing for water resources management: Potential for supporting sustainable development in data-poor regions. *Water Resources Research*, 54(12), 9724-9758.

Soncini, A., Bocchiola, D., Confortola, G., Minora, U., Vuillermoz, E., Salerno, F., & Diolaiuti, G. (2016). Future hydrological regimes and glacier cover in the Everest region: The case study of the upper Dudh Koshi basin. *Science of the Total Environment*, 565, 1084-1101.

Sorg, A., Bolch, T., Stoffel, M., Solomina, O., & Beniston, M. (2012). Climate change impacts on glaciers and runoff in Tien Shan (Central Asia). *Nature Climate Change*, 2(10), 725-731.

Tang, Q., Gao, H., Lu, H., & Lettenmaier, D. P. (2009). Remote sensing: hydrology. *Progress in Physical Geography*, 33(4), 490-509.

Taylor, R. G., Scanlon, B., Döll, P., Rodell, M., Van Beek, R., Wada, Y., & Konikow, L. (2013). Ground water and climate change. *Nature climate change*, 3(4), 322-329.

Tedesco, M., Kelly, R., Foster, J. L., & Chang, A. T. C. (2004). AMSR-E/aqua daily L3 global snow water equivalent EASE-grids. Version 2. AE_DySno. Boulder, Colorado USA. *NASA National Snow and Ice Data Center Distributed Active Archive Center*.

Valt, M., Guyennon, N., Salerno, F., Petrangeli, A. B., Salvatori, R., Cianfarra, P., & Romano, E. (2018). Predicting new snow density in the Italian Alps: A variability analysis based on 10 years of measurements. *Hydrological Processes*, 32(20), 3174-3187.

Veloso, A., Mermoz, S., Bouvet, A., Le Toan, T., Planells, M., Dejoux, J. F., & Ceschia, E. (2017). Understanding the temporal behavior of crops using Sentinel-1 and Sentinel-2-like data for agricultural applications. *Remote sensing of environment*, 199, 415-426.

Viviroli, D., Dürr, H. H., Messerli, B., Meybeck, M., & Weingartner, R. (2007). Mountains of the world, water towers for humanity: Typology, mapping, and global significance. *Water resources research*, 43(7).

West, H., Quinn, N., & Horswell, M. (2019). Remote sensing for drought monitoring & impact assessment: Progress, past challenges and future opportunities. *Remote Sensing of Environment*, 232, 111291.

Wilson, J. L., & Guan, H. (2004). Mountain-block hydrology and mountain-front recharge. *Groundwater recharge in a desert environment: The Southwestern United States*, 9.

Zhang, K., Kimball, J. S., & Running, S. W. (2016). A review of remote sensing based actual evapotranspiration estimation. *Wiley Interdisciplinary Reviews: Water*, 3(6), 834-853.